Contribution to the Calculation of the Linear and Non-Linear Behaviour of Hingeless Rotor Blades with Uneven Blade Properties
- A Simple Calculation Tool -

A.Büter and U.-C. Ehlert
German Aerospace Research Establishment (DLR), Institute of Structural Mechanics
Lilienthalplatz 7, 38108 Braunschweig, Germany
Tel.: +49 531/295 2317; E-Mail: andreas.bueter@dlr.de

F. Nitzsche
Carleton University, Mechanical and Aerospace Engineering
1125 Colonel By Drive, Ottawa, ON K1S 5B6 Canada

ABSTRACT

This paper deals with a simple tool for the calculation of the linear and non-linear behaviour of hingeless rotor blades with uneven blade properties. The calculation is based on the Galerkin Method which is used for solution of the non-linear differential equations given by Hodges and Dowell [1] and aims at the fan diagram or rotor design, respectively.

After a physical interpretation of the coupled differential equations, the basis of the calculation tool is described. The calculation is divided into two steps: In step one the linear system of differential equations is solved by a numerical solver based on the Integration Matrix Method [2],[3],[4],[5]. The resulting static and dynamic deflections of the “linear“ rotor blade are the inputs for the second part, in which the non-linear differential equations is then solved by the Galerkin Method.

1. LIST OF SYMBOLS

A : surface of the cross-section (blade) [m²]
e : mass centroid offset from elastic axis [m]
EA’ : elongation stiffness per unit [N]
$EI_{y'}$: bending stiffness per unit (flap) [Nm²]
$EI_{z'}$: bending stiffness per unit (lead-lag) [Nm²]
F_{QL} : shear force (lead-lag) [Nm]
F_{QF} : shear force (flap) [Nm]
GJ : torsional stiffness per unit [Nm²]
H : torsional moment [Nm]
$I_{y'}$: cross-section moment of inertia (F) [m⁴]
$I_{z'}$: cross-section moment of inertia (LL) [m⁴]
I_{β}' : inertia mass per unit (flap) [kg m²]
I_{γ}' : inertia mass per unit (lead-lag) [kg m²]
I_{θ}' : inertia mass per unit (torsion) [kg m²]
$K_{\phi u}$: coupling stiffness per unit (tension-torsion)
m’ : mass per unit length [kg/m]
M_{bL} : bending moment (lead-lag) [Nm]
M_{bF} : bending moment (flap) [Nm]
P : tension force [N]
R : rotor blade radius [m]
u : elongation [m]
v : bending deformation (lead-lag) [m]
w : bending deformation (flap) [m]

x,y,z : coordinate system axes (rotor)
x’,y’,z’ : coordinate system axes (blade)

β : slope (flap) [-]
γ : slope (lead-lag) [-]
ϕ : torsional deflection [rad]
θ : blade twist angle (fix) [rad]
ω : frequency [1/sec]
Ω : revolution per minute [rpm]

2. INTRODUCTION

Present helicopter research mainly focuses on the improvement of the aerodynamic efficiency and on the reduction of vibrations and acoustic emissions. A direct approach is aiming at the physical sources of these problems. This can be reached by adaptive structural technology.

In general, helicopter vibrations and noise exist in all flight cases mainly due to the unsteady working conditions of the blade. This results from interactions between the highly non-stationary aerodynamics induced by the rotating rotor blades and special aerodynamic phenomena like the stall effect at the retreating blade and the transonic effect at the advancing blade. All these vibrations are of a highly dynamic nature [6]. The Blade Vortex Interaction (BVI) phenomenon in descend flight is extremely penalising as far as external noise is concerned
The comprehension of this relationship between the aerodynamic sources and the resulting vibrations and noise is the basis for optimally designed control concepts. Special emphasis is placed on the opti-

misation of the standard blade control and active control of the blade deflection as the primary tools.

All aerodynamic effects react very sensitive to small variations of angle of attack and inflow velocity. Therefore, the main idea of the measures, which aims at the reduction of vibrations and acoustic emission, is to dynamically change the blade pitch (twist) or the rotor blade characteristics. Different means are considered for this, e.g. adaptive blade twist, deformable airfoil sections or additional trailing edge flaps.

In [8] it has been shown that adaptive blade twist based on torsion-tension-coupling is a usable concept for adaptive rotor blades. In general, torsion-tension-coupling is an anisotropic behaviour which appears in structural components. It can be realised by orientated stiffness. In this concept anisotropic material behaviour caused by helical winding is illustrated in figure 1. The principle of this actuator concept is presently being developed at the DLR. [5], [7], [8]

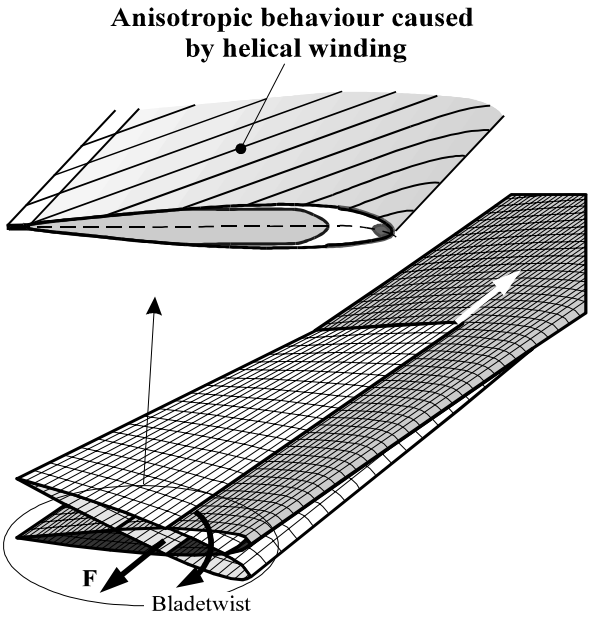

Figure 1: Adaptive blade twist

For practical realisation, cylindrical actuators like piezoelectric elongators (piezo-stacks) integrated in the rotor blade structure will be used. The actuator is a discrete mass which changed the uneven blade properties and the dynamic behaviour of the hingeless rotor dramatically. Therefore, to realise a efficient adaptive rotor system, a calculation of the *Fan-Diagram* and a final rotor design is necessary. Based on the present rotor blade, the rotor design aims at the mathematical assessment of the ideal uneven stiffness and mass distribution for the active blade.

This paper deals with a simple tool for such calculations of linear and non-linear behaviour of hingeless rotor blades with uneven blade properties.

3. Physical Interpretation of the Coupled Differential Equations

The following calculations are based on the *Non-linear Equations of Motion for the Elastic Bending and Torsion of Twisted Nonuniform Rotor Blades* given by Hodges/Dowell [1]. In these equations the aerodynamic forces, precone angle and the area centroid offset from elastic axis are equal to zero. The independent variables are the spanwise coordinate r and time. Dots denote the time differentiation and primes the spatial differentiation.

Elongation (U):

$$0 = -P' + m'\ddot{u} - \Omega^2 m' r - 2\Omega m' \dot{v} \qquad (1)$$

Lead-Lag (LL):

$$0 = \{P v'\}' + \{BL1\, v'' + BFL\, w''\}'' + m' \ddot{v} - m' e \sin\theta \ddot{\phi}$$
$$- \{\Omega^2 m' r e (\sin\theta \phi - \cos\theta) - 2\Omega m' e \cos\theta \dot{v}\}'$$
$$- \Omega^2 m' v + 2\Omega m' \dot{u} - 2\Omega m' e (\dot{v}' \cos\theta + \dot{w}' \sin\theta) \qquad (2)$$

Flap (F):

$$0 = \{P w'\}' + \{BF1\, w'' + BFL\, v''\}'' + m' \ddot{w} + m' e \cos\theta \ddot{\phi}$$
$$+ \{\Omega^2 m' r e (\cos\theta \phi + \sin\theta) - 2\Omega m' e \sin\theta \dot{v}\}' \qquad (3)$$

Torsion (T):

$$0 = \{K_A^2 (\theta' + \phi') P - GJ \phi' + K_{\phi u} u'\}' - I_\theta' \ddot{\theta}$$
$$+ \Omega^2 K_{md}^2 (\cos 2\theta \phi + \cos\theta \sin\theta)$$
$$+ (EI_z' - EI_y') \cos\theta \sin\theta (v''^2 - w''^2)$$
$$+ (EI_z' - EI_y') \cos 2\theta\, v'' w'' - m' e (\cos\theta \ddot{w} - \sin\theta \ddot{v})$$
$$+ \Omega^2 m' r e (\cos\theta w' - \sin\theta v') + \Omega^2 m' e \sin\theta v \qquad (4)$$

where

$$P = EA \left(u' + \frac{w'^2}{2} + \frac{v'^2}{2} + K_A^2 \theta' \phi' \right) + K_{\phi u} \phi' \qquad (5)$$

With the identities

$$BF1 = [EI_y' + (EI_z' - EI_y') \sin^2\theta]$$

$$BL1 = [EI_z' - (EI_z' - EI_y') \sin^2\theta]$$

$$BFL = (EI_z' - EI_y') \sin 2\theta$$

$$K_A = \sqrt{\frac{I_y' + I_z'}{A}}$$

$$K_{md} = I_\beta' - I_\gamma'$$

Equation (5) describes the internal tension forces in the blade due to the elastic deformation. The external tension forces can derived from equation (1).

$$P = \int_r^R m'(x) \ddot{u}(x)\, dx - \Omega^2 \int_r^R m'(x)\, r\, dx - 2\Omega \int_r^R m'(x)\, \dot{v}(x)\, dx$$

Inserted in equation (2) and (3), the physical interpretation of the components {P w'}' and {P v'}' becomes clear. They describe the flap and lead-lag shear force distribution due to the inertial, centrifugal and coriolis forces. In this the most significant component is given by the centrifugal force, wherein the effective lead-lag and flapwise bending stiffness dramatically increase with the rotation speed Ω.
In table 1 the physical interpretations for all components of the differential equation system are listed.

Inertial forces (U, LL, F, T)	$m' \ddot{u}$; $m' \ddot{v}$; $m' \ddot{w}$; $I_\theta' \ddot{\phi}$
Centrifugal forces (U)	$\Omega^2 m' r$
Shear force due to centrifugal forces on the with v deflected blade (LL)	$\Omega^2 m' v$
Coriolis forces (U, LL)	$2\Omega m' \dot{v}$; $2\Omega m' \dot{u}$
Stiffness forces - unsymmetrical bending (LL, F)	$\{BL1\ v'' + BFL\ w''\}''$ $\{BF1\ w'' + BFL\ v''\}''$
Stiffness forces - tension-torsion-coupling (U, T)	$\{EA\ u' + K_{\phi u}\ \phi'\}'$ $\{GJ\ \phi' + K_{\phi u}\ u'\}'$
Bending and torsional moments due to different tension forces e.g. centrifugal, coriolis and inertial force (LL, F, T)	$\{P\ v'\}'$ $\{P\ w'\}'$ $\{K_A^2\ (\theta' + \phi')\ P\}'$
Shear force and torsional moment distribution (LL, F, T) Bending-torsion-coupling due to inertial forces!	$-\ m' e \sin\theta\ \ddot{\phi}$ $m' e \cos\theta\ \ddot{\phi}$ $-\ m' e (\cos\theta\ \ddot{w} - \sin\theta\ \ddot{v})$
Bending and torsional moments due to the centrifugal forces (LL, F, T) Bending-torsion-coupling due to centrifugal forces!	$-\{\Omega^2 m' r e (\sin\theta\ \phi - \cos\theta)\}'$ $\{\Omega^2 m' r e (\cos\theta\ \phi + \sin\theta)\}'$ $\Omega^2 m' r e (\cos\theta\ w' - \sin\theta\ v')$
Bending moments due to the coriolis forces (F, LL)	$\{2\Omega m' e \cos\theta\ \dot{v}\}'$ $-\{2\Omega m' e \sin\theta\ \dot{v}\}'$
Bending curvature induced torsional moment (T)	$(EI_{z'} - EI_{y'}) \cos\theta \sin\theta\ v''^2$ $-(EI_{z'} - EI_{y'}) \cos\theta \sin\theta\ w''^2$ $+ (EI_{z'} - EI_{y'}) \cos 2\theta\ v''\ w''$
Propeller moment (T)	$\Omega^2 K_{md}^2 \cos 2\theta\ \phi$ $+ \Omega^2 K_{md}^2 \cos\theta \sin\theta)$

Table 1: Physical interpretations for the components in the differential equations system

The non-linear components (underlined) of the differential equation system are the curvature induced torsion and parts of the bending and torsional moments caused by tension forces. Especially the bending moments due to the coriolis forces and the inertial force are non-linear components in the lead lag and flap motion equations.

4. Galerkin-Method for Linear and Non-Linear Rotor Blade Calculations

The above mentioned non-linear differential equations can be solved by the Galerkin Method.

In the following representations of displacements:

Elongation: $$u(r) = \sum_{i=1}^{n} (U_{oi} + \Delta U_i)\ u_i(r)$$

Lead-Lag: $$v(r) = \sum_{i=1}^{n} (V_{oi} + \Delta V_i)\ v_i(r)$$

Flap: $$w(r) = \sum_{i=1}^{n} (W_{oi} + \Delta W_i)\ w_i(r)$$

Torsion: $$\phi(r) = \sum_{i=1}^{n} (\Phi_{oi} + \Delta \Phi_i)\ t_i(r)$$

the shape functions $u_i(r)$, $v_i(r)$, $w_i(r)$ and $t_i(r)$, which describe the possibilities of rotor blade deformations, have to be chosen with a mechanical preknowledge of the results. Especially the geometric and dynamical boundary conditions must be fulfilled by these functions. The number and quality of these functions correlate directly with the precision of results and determine the degrees of freedom which can be calculated. U_{oi}, V_{oi}, W_{oi} and Φ_{oi} are the „weighting factors" of the shape functions for the static and ΔU_i, ΔV_i, ΔW_i and $\Delta \Phi_i$ for the dynamic blade deformation.

With these representations of displacements, the complicated two-dimensional problem can be converted into a non-linear equation system to evaluate the static deformations of the rotor blades and to solve classic eigenvalue problem to get the modal parameters (eigenvalues, modeshapes and damping) of such deformed rotor blades.

After introducing the description for the displacements in the Ritz-Galerkin energy equations

Elongation: $$0 = \int_0^R u_m(r)\ U(u, v, w, t)\ dr \qquad (6)$$

Lead-Lag: $$0 = \int_0^R v_m(r)\ LL(u, v, w, t)\ dr \qquad (7)$$

Flap: $$0 = \int_0^R w_m(r)\ F(u, v, w, t)\ dr \qquad (8)$$

Torsion: $$0 = \int_0^R t_m(r)\ T(u, v, w, t)\ dr \qquad (9)$$

with

U, LL, F, T: Differential equations for elongation (U), lead-lag, flap and torsion
u, v, w, t: Description for the displacements
m = 0, ..., n

a system of a non-linear equations is derived to evaluate the static deformations and homogeneous differential equation system and to obtain the modal parameters.

Based on the above mentioned procedure a flexible calculation tool suitable for the Personal Computer was developed, shown in figure 2. In order to evaluate the influence of the shape functions and non-linear components in the differential equations, the input database and the calculation flow must be controllable for the user.

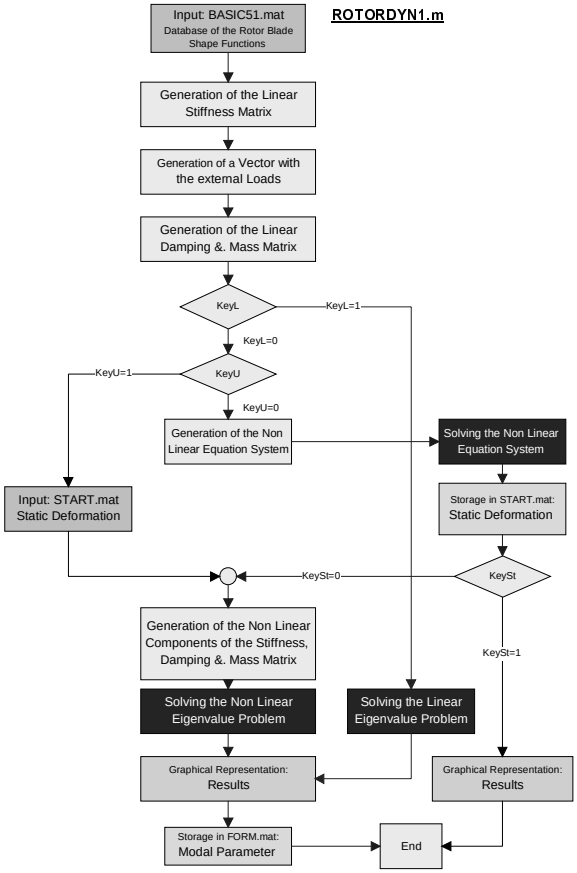

Figure 2: Flow diagram of the calculation tool to solve the linear or non-linear system by the Galerkin-method

The final goal is to build a *simple* tool for the calculation of hingeless rotor blades with uneven blade properties. This tool aims at the fan diagram or rotor design, respectively.

There are two possibilities for simplification:

1st - The reduction of the system complexity e.g. to solve only the equation system with linear behaviour.

2nd - The reduction of the number of shape functions, e.g. due to more suitable shape functions. These shape functions may be derived from the linear motion equations and calculated by a numerical tool described in the next chapter.

To evaluate the efficiency of these two possibilities, first the above mentioned *flexible* calculation tool based on the Galerkin Method is needed. Within this tool a solution of the linear or non-linear motion equations is possible for a various number of shape functions.
Secondly, a *simple* numerical tool is required to solve the linear motion equations. The results of this calculations i.e. the normalized mode shapes and static deformations are the input for the Galerkin Method. In the following such a *simple* numerical tool will be described.

5. Hybrid State Vector Method for Linear Rotor Blade Calculations

For the Hybrid State Vector Method or Integration-matrix Method the linear blade motion equations (1) - (4) are cast in a state vector form.

Elongation:

$$P' = m' \ddot{u} - \Omega^2 m' r - 2\Omega m' \dot{v} \tag{10}$$

$$u' = U_{11} P + U_{12} H \tag{11}$$

Lead-Lag:

$$M_{bL}' = - F_{QL} - \Omega^2 \int_r^R m' x \, dx \, \gamma + 2\Omega m' e \cos\theta \, \dot{v} - \Omega^2 m' r e (\sin\theta \, \phi - \cos\theta) \tag{12}$$

$$F_{QL}' = m' \ddot{v} - m' e \sin\theta \, \ddot{\phi} + \Omega^2 m' r (\sin\theta \, \phi - \cos\theta) + 2\Omega m' \dot{u} - \Omega^2 m' v - 2\Omega m' e (\dot{\gamma} \cos\theta + \dot{\beta} \sin\theta) \tag{13}$$

$$v' = \gamma \tag{14}$$

$$\gamma' = K_V M_{bL} - K_{VW} M_{bF} \tag{15}$$

Flap:

$$M_{bF}' = - F_{QF} + \Omega^2 \int_r^R m' x \, dx \, \beta - 2\Omega m' e \sin\theta \, \dot{v} + \Omega^2 m' r e (\cos\theta \, \phi + \sin\theta) \tag{16}$$

$$F_{QF}' = m' \ddot{w} + m' e \cos\theta \, \ddot{\phi} \tag{17}$$

$$w' = - \beta \tag{18}$$

$$\beta' = K_W M_{bF} - K_{VW} M_{bL} \tag{19}$$

Torsion:

$$H' = - I_\theta' \ddot{\phi} + \Omega^2 K_{md}^2 (\cos 2\theta \, \phi + \cos\theta \sin\theta) + K_A^2 \theta' P - e m' (\cos\theta \, \ddot{w} - \sin\theta \, \ddot{v}) + \Omega^2 m' r e (\cos\theta \, \beta - \sin\theta \, \gamma) + \Omega^2 m' e \sin\theta \, v \tag{20}$$

$$\phi' = U_{12}\, P + U_{22}\, H \qquad (21)$$

with

$ey = [EI_y' \cos^2\theta + EI_z' \sin^2\theta]$

$ez = [EI_z' \cos^2\theta + EI_y' \sin^2\theta]$

$eyz = (EI_z' - EI_y') \sin\theta \cos\theta$

$$K_v = \frac{ey}{ey\ ez - eyz^2}$$

$$K_w = \frac{ez}{ey\ ez - eyz^2}$$

$$K_{vw} = \frac{eyz}{ey\ ez - eyz^2}$$

$$U_{11} = \frac{GJ}{EA\ GJ - K_{\phi u}^2}$$

$$U_{22} = \frac{EA}{EA\ GJ - K_{\phi u}^2}$$

$$U_{12} = \frac{K_{\phi u}^2}{EA\ GJ - K_{\phi u}^2}$$

This set of 12 first order differential equations may be discretized in space by defining the blade local properties as elements of diagonal matrices of dimension N.

After normalisation, discretisation and integration described in Appendix A and considering the boundary conditions:

$u(0) = 0$;	$P(R) = 0$;
$v(0) = 0$;	$F_{QL}(R) = 0$;
$\gamma(0) = 0$;	$M_{bL}(R) = 0$;
$w(0) = 0$;	$F_{QF}(R) = 0$;
$\beta(0) = 0$;	$M_{bF}(R) = 0$;
$\phi(0) = 0$ and	$H(R) = 0$

the following only time-varying differential equation system can be obtained:

$$\mathbf{P} = -R\,\mathbf{L_o}\,\mathbf{m'}\,\ddot{\mathbf{u}} + 2\Omega R\,\mathbf{L_o}\,\mathbf{m'}\,\dot{\mathbf{v}} + \Omega^2 R\,\mathbf{L_o}\,\mathbf{m'}\,\mathbf{r}$$

$$\mathbf{u} = R\,\mathbf{L}\,\mathbf{U_{11}}\,\mathbf{P} + R\,\mathbf{L}\,\mathbf{U_{12}}\,\mathbf{H}$$

$$\mathbf{M_{bL}} = R\,\mathbf{L_o}\,\mathbf{F_{QL}} - R\,\mathbf{L_o}\,\mathbf{T}\,\gamma - 2\Omega R\,\mathbf{L_o}\,\mathbf{m'}\,\mathbf{e}\cos\theta\,\dot{\mathbf{v}} + \Omega^2 R\,\mathbf{L_o}\,\mathbf{m'}\,\mathbf{r}\,\mathbf{e}\,(\sin\theta\,\phi - \cos\theta)$$

$$\mathbf{F_{QL}} = -R\,\mathbf{L_o}\,\mathbf{m'}\,\ddot{\mathbf{v}} - \Omega^2 R\,\mathbf{L_o}\,\mathbf{m'}\,\mathbf{r}\,(\sin\theta\,\phi - \cos\theta) + R\,\mathbf{L_o}\,\mathbf{m'}\,\mathbf{e}\sin\theta\,\ddot{\phi} - 2\Omega R\,\mathbf{L_o}\,\mathbf{m'}\,\dot{\mathbf{u}} + \Omega^2 R\,\mathbf{L_o}\,\mathbf{m'}\,\mathbf{v} + 2\Omega R\,\mathbf{L_o}\,\mathbf{m'}\,\mathbf{e}\,(\dot{\gamma}\cos\theta + \dot{\beta}\sin\theta)$$

$$\mathbf{v} = R\,\mathbf{L}\,\gamma$$

$$\gamma = R\,\mathbf{L}\,\mathbf{K_v}\,\mathbf{M_{bL}} - R\,\mathbf{L}\,\mathbf{K_{vw}}\,\mathbf{M_{bF}}$$

$$\mathbf{M_{bF}} = -R\,\mathbf{L_o}\,\mathbf{F_{QF}} - R\,\mathbf{L_o}\,\mathbf{T}\,\beta + 2\Omega R\,\mathbf{L_o}\,\mathbf{m'}\,\mathbf{e}\sin\theta\,\dot{\mathbf{v}} - \Omega^2 R\,\mathbf{L_o}\,\mathbf{m'}\,\mathbf{r}\,\mathbf{e}\,(\cos\theta\,\phi + \sin\theta)$$

$$\mathbf{F_{QF}} = -R\,\mathbf{L_o}\,\mathbf{m'}\,\ddot{\mathbf{w}} - R\,\mathbf{L_o}\,\mathbf{m'}\,\mathbf{e}\cos\theta\,\ddot{\phi}$$

$$\mathbf{w} = -R\,\mathbf{L}\,\beta$$

$$\beta = -R\,\mathbf{L}\,\mathbf{K_w}\,\mathbf{M_{bF}} - R\,\mathbf{L}\,\mathbf{K_{vw}}\,\mathbf{M_{bL}}$$

$$\mathbf{H} = -R\,\mathbf{L_o}\,\mathbf{I_\theta'}\,\ddot{\phi} + \Omega^2 R\,\mathbf{L_o}\,\mathbf{K_{md}^2}\,(\cos2\theta\,\phi + \cos\theta\sin\theta) + R\,\mathbf{L_o}\,\mathbf{K_A^2}\,\theta'\,\mathbf{P} - R\,\mathbf{L_o}\,\mathbf{m'}\,\mathbf{e}(\cos\theta\,\ddot{\mathbf{w}} - \sin\theta\,\ddot{\mathbf{v}}) + \Omega^2 R\,\mathbf{L_o}\,\mathbf{m'}\,\mathbf{r}\,\mathbf{e}\,(\cos\theta\,\beta - \sin\theta\,\gamma) + \Omega^2 R\,\mathbf{L_o}\,\mathbf{m'}\,\mathbf{e}\sin\theta\,\mathbf{v}$$

$$\phi = R\,\mathbf{L}\,\mathbf{U_{12}}\,\mathbf{P} + R\,\mathbf{L}\,\mathbf{U_{22}}\,\mathbf{H}$$

where $\mathbf{L_o}$ and $\mathbf{T}$ defined by

$$\mathbf{L_o} = (\mathbf{B_1} - \mathbf{I})\mathbf{L}$$

$$T = \Omega^2 R\,\mathbf{L_o}\,\mathbf{m'}\,\mathbf{r}\ .$$

In frequency domain this time-varying differential equation system becomes a linear equation system. The programme wherein these equations can be solved is shown in figure 3.

The fan-diagram, static deformations and mode shapes of the rotor system can be calculated by this tool. The advantage is a closed numerical solution of the linear motion equations.
Based on these opportunities the evaluation of the influence of the shape functions and non-linear components in the differential equations is possible.

To show the conformity of this calculation tool with analytical solutions in two special cases, computations based on a non-rotating, uncoupled beam with even properties and a constant shear force distribution were made. The analytical solutions were calculated with

$$w(x) = \frac{10\ l^4}{24\ EI_y'}\left(6\frac{x^2}{l^2} - 4\frac{x^2}{l^2} + \frac{x^4}{l^4}\right) \qquad \text{(Flap)}$$

$$v(x) = \frac{100\ l^4}{24\ EI_z'}\left(6\frac{x^2}{l^2} - 4\frac{x^2}{l^2} + \frac{x^4}{l^4}\right) \qquad \text{(Lead-Lag)}$$

wherein

$EI_y' = 250$ [Nm²] , $EI_z' = 5200$ [Nm²] , $l = 0{,}76$ m [m] .

The courses of deformation and the deformations at the beam tip are equal in both cases. Therefore, the results of FORM2.m are defined as the reference case for the following calculation.

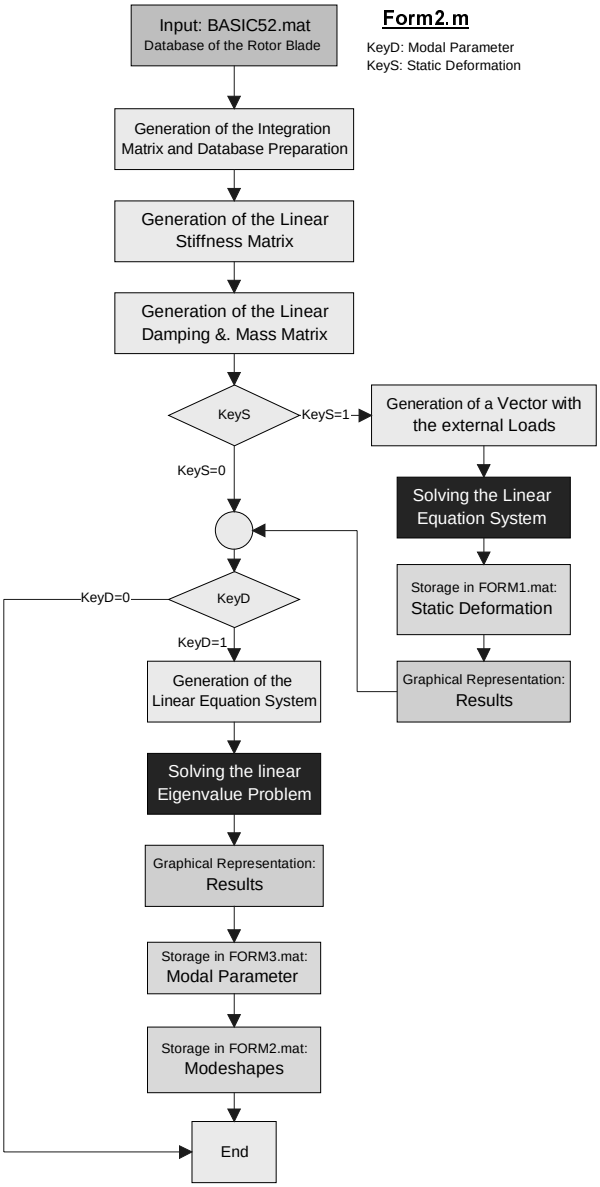

Figure 3: Flow diagram of the calculation tool to solve the linear system by the integration matrix method.

6. SENSITIVITY OF RESULTS

In figure 4 the normalised static deformations, the 1st and 2nd mode shapes for different rotational velocities and bending motions calculated by FORM2.m are shown. The course of the deformation depends on the different uneven blade properties for flapwise and lead-lag bending as well as the changing type of loads. The different blade properties cause, and the course of deformations, whereas the changed types of loads influence.

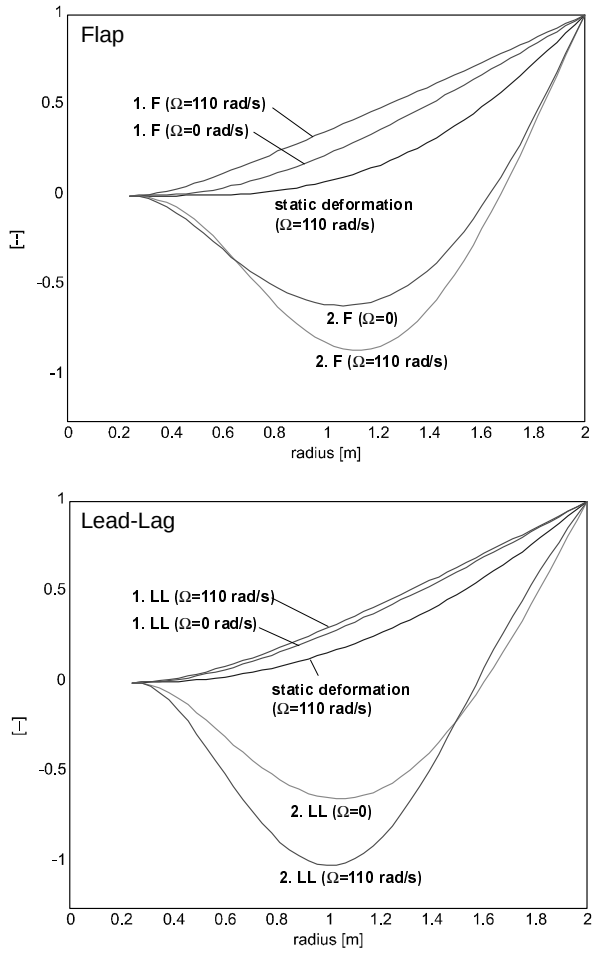

Figure 4: The normalized static deformation, the 1st and 2nd mode shapes for different rotational velocities and bending motions (uneven blade properties).

The idea of the Galerkin-Method is to rebuild these different courses of deformation by a superposition of many weighted independent shape functions. It seems to be logical that the number of required shape functions decreases, if they are similar to the real deformation functions of the rotor blade.
To assess the influence of the chosen shape functions and the non-linear components of the differential equation four calculations were made:

- ROTORDYN1.m - linear, shape functions given in [10] for even blade properties - **(1)**
- FORM2.m - linear - **(2)**
- ROTORDYN1.m - linear, shape functions from FORM 2.m - **(3a)**
- ROTORDYN1.m - non-linear, shape functions from FORM 2.m - **(3b)**

The database for these calculations is given by a pretwisted model rotor blade with uneven blade properties. The smoothed blade properties are shown in appendix B.

With FORM2.m shape functions similar to the real deformation functions of the rotor blade were calculated. For the calculations with ROTORDYN1.m (Galerkin Method) eight shape functions for each type of motion (U, LL, F and T), i.e. a set of 32 shape functions is directly derived from [10] for rotor blades with even blade properties (figure 5) and used for calculation (1).

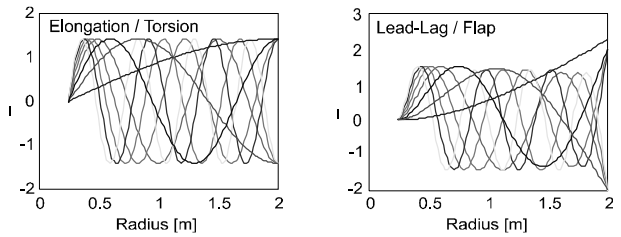

Figure 5: Shape functions given by [10] **for even blade properties - (1)**

A second of 32 shape functions was chosen for calculations (3a) and (3b). This second set was based on the first set; only 10 shape functions, i.e. the

- first for the elongation,
- first and second for the torsion,
- first, second and third for the lead-lag,
- first, second, third and forth for the flap

are exchanged by the ones calculated with FORM2.m. In figure 6 the shape functions for each motion are shown.

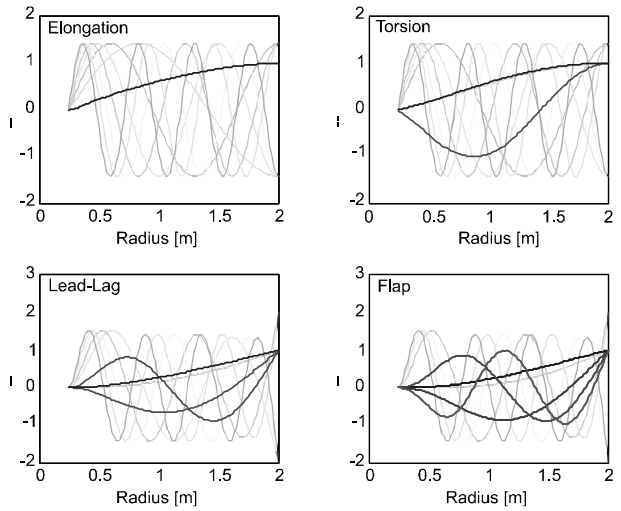

Figure 6: Shape functions - (3a) and (3b)

The calculations include the blade tip deformations for the maximal rotational velocity, the eigenvalues and the fan diagrams.

The blade tip deformations for the maximal rotational velocity calculated with the different tools are shown in table 2.

	(1)	(2)	(3b)
static	**110 rad/s**	**110 rad/s**	**110 rad/s**
u(R)	1,8 mm	3,2 mm	3,3 mm
v(R)	19,6 mm	–9,5 mm	–8,3 mm
w(R)	–1,4 mm	0,6 mm	0,6 mm
ϕ(R)	0,18°	0,2°	0,57°

Table 2: Static blade tip deformation for the maximal rotational velocity calculated with the different tools (uneven blade properties).

A comparison of these results shows the influence of the shape functions and of the non-linear components in the differential equation. Especially the latter essentially influence the static torsional and lead-lag deflection. With the 32 shape functions derived from [10] (1) it is not possible to calculate the blade tip deflections with sufficient precision as compared to (2). Even changes of sign (v, w) occur. The calculated eigenvalues, listed in table 3, show the same behaviour.

(1)	(2)	(3a)	(3b)
0 rad/s	**0 rad/s**	**0 rad/s**	**0 rad/s**
4,5 Hz	2,7 Hz	3,0 Hz	3 Hz
17,6 Hz	11,1 Hz	12 Hz	12 Hz
27,3 Hz	16 Hz	17 Hz	17,1 Hz
71,5 Hz	41,8 Hz	43,8 Hz	44,4 Hz
93,2 Hz	69,1 Hz	69,3 Hz	72,0 Hz
118,3 Hz	69,9 Hz	75,9 Hz	75,8 Hz

(1)	(2)	(3a)	(3b)
110 rad/s	**110 rad/s**	**110 rad/s**	**110 rad/s**
27,2 Hz	15,2 Hz	15,9 Hz	15,9 Hz
28,5 Hz	20,3 Hz	19,8 Hz	19,8 Hz
68,4 Hz	49,2 Hz	51,0 Hz	51,1 Hz
95,5 Hz	72,1 Hz	72,1 Hz	74,7 Hz
122,6 Hz	81,1 Hz	85,5 Hz	85,9 Hz
132,6 Hz	86,8 Hz	90,6 Hz	90,6 Hz

Table 3: Eigenvalues for different rotational velocities calculated with the different tools (uneven blade properties).

(1) ROTORDYN1.m (linear, shape functions derived from [10] for even blade properties)
(2) FORM2.m (linear)
(3a) ROTORDYN1.m (linear, shape functions derived from FORM 2.m)
(3b) ROTORDYN1.m (non-linear, shape functions derived from FORM 2.m)

In comparison to the results of FORM2.m (2) it is not possible to calculate the eigenvalues with the shape functions derived from [10] with sufficient precision. The calculations with modified shape functions (3a),(3b) shows better results. Better still there are differences between the higher eigenvalues in comparison to the results of FORM2.m. To improve these results, the number of exchanged shape function must be increased.

In figure 7, 8 and 10 the fan diagrams calculated with the different tools are shown. The differences in

value and course of the higher eigenvalues is visible too.

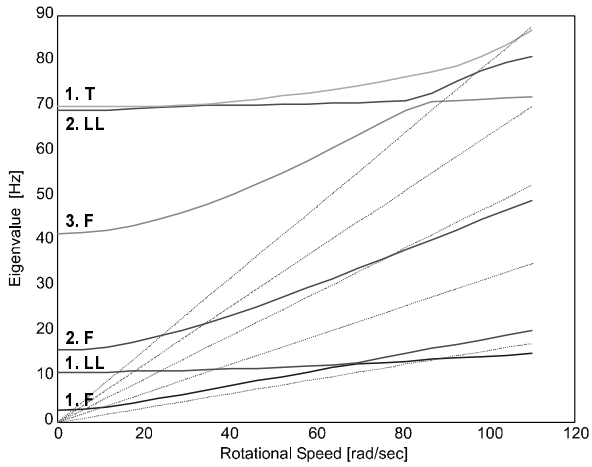

Figure 7: Fan diagram calculated with FORM2.m - (2)

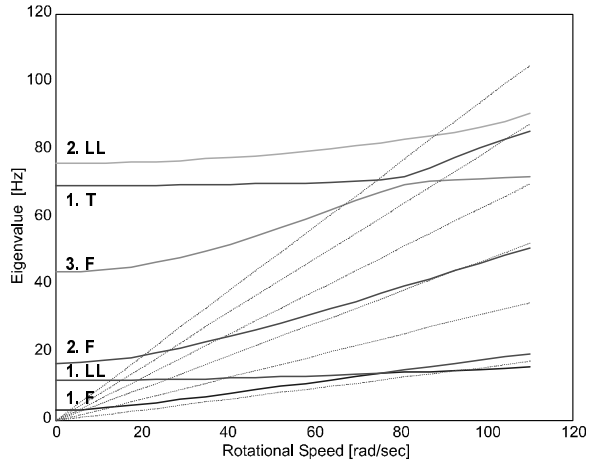

Figure 8: Fan diagram calculated with ROTORDYN1.m - (3a)

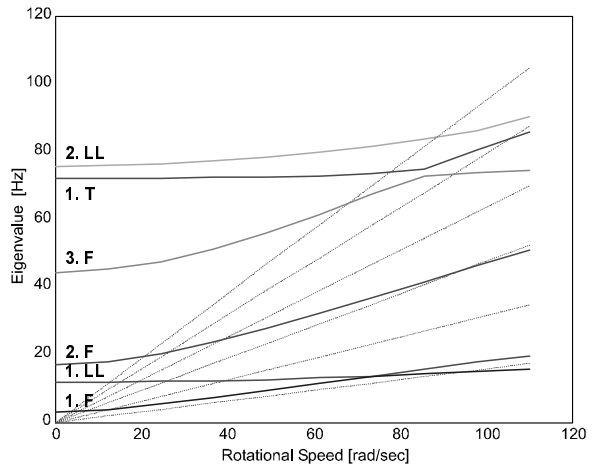

Figure 9: Fan diagram calculated with ROTORDYN1.m - (3b)

7. CONCLUSIONS AND OUTLOOK

The results can be improved by using of shape functions similar to the real deformation functions of the rotor blade. The number of these precalculated shape functions define the number of eigenvalues, which computed correctly. Therefore, to evaluate the higher eigenvalues, e.g. for flap and lead-lag, the number of exchanged shape functions needs to be increased.

It was shown that the real deformation functions depend on the blade properties and the load distribution. These load distributions change with the rotational speed, so that for further calculations, especially to get a fan diagram, the shape functions could be changed with the rotational speed. This seems quiet complicated, but the increase of the number of shape functions consumes more computation time per calculation cycle than the precalculations of new shape functions.

Finally, it was shown that the differences between the solution from the linear and non-linear equations allow us, to use the much simpler linear tools for the preliminary rotor design. Only for final calculations tools based on non-linear equations should be used.

8. REFERENCES

[1] Hodges, D.H. ; Dowell, E.H.: *Non-linear Equations of Motion for the Elastic Bending and Torsion of Twisted Nonuniform Rotor Blades,* NASA Technical Note, NASA TN D-7818, December 1974

[2] Lehmann, Larry L.: *Hybrid State Vector Methods for Structural Dynamic and Aeroelastic Boundary Value Problems*, NASA Contractor Report 3591, August 1982

[3] Lehmann, Larry L.: *Integration Matrix Solution of the Hybrid State Vector Equations for Beam Vibration*, 23. SDM Conference, 1982 New Orleans, LA

[4] Nitzsche, F.: AIAA-93-1703: *Modal Sensors and Actuators for Individual Blade Control.* 34. SDM Conference, Adaptive Structure Forum, 1993 La Jolla, CA

[5] Büter,A.: *Untersuchung adaptiver Konzepte zur Reduktion von Hubschraubervibrationen, zur Minderung des Hubschrauberlärms und zur Steigerung der aerodynamischen Effizienz*, Dissertation an der RWTH Aachen, DLR Forschungsbericht 98-12, Juni 1998

[6] Bielawa,R.L.: *Rotary Wing Structural Dynamics and Aeroelasticity*, AIAA Education Series 1992.

[7] Büter,A.; Piening,M.: *Verdrehbares Rotorblatt aus faserverstärktem Kunstharz*, Deutsches Patent Aktenzeichen 195 28 155.1 (1995)

[8] Büter,A.; Breitbach,E.: *Adaptive Blade Twist - Calculations and Experimental Results*, AST Aerospace Science and Technology, Page 309-319, Heft 4, 2000

[9] Nitzsche, F.: AIAA-92-2452: *A Study on the Feasibility of Using Adaptive Structures in the Attenuation of Vibration Characteristics of Rotary Wings.* 33. SDM Conference, Adaptive Structure Forum, 1992 Dallas, TX

[10] Chang, T.-C., Craig, Jr., R. R.: *On Normal Modes of Uniform Beams.* EMRL 1068, 1969

9. APPENDIX A - INTEGRATING MATRIX

The description based on [9]. A better description of the method may be found in [2], [3] and [4].

The boldfaced letters denotes vectors or matrices.

The function f(x) is a dimensionless function defined in the interval 0,1 and discretized in N grid point i.e. in N-1 subintervals. (Figure A.1)

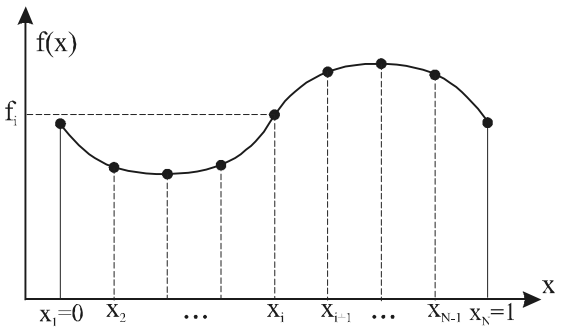

Figure A.1

Assuming that f(x) can be approximated by a n-th degree polynomial in the i-th subinterval an integration of f(x) over such a subinterval would appear as:

$$\int_{x_i}^{x_{i+1}} f(x)\,dx \approx \sum_{k=j}^{k=j+n} W_{ik} \cdot f_k \qquad (n \le N+1 \text{ and } i=1,..,N-1)$$

where W_{ik} are weighting numbers that are independent of the value of the function. The integer j is the starting point of a general sequence of consecutive n+1 grid points at which the function is approximated by the n-th degree polynomial ($1 \le j \le N-n$). Defining the vector:

$$\mathbf{f} = [f_1, f_2, f_3, \ldots, f_N]^T_{N\times 1}$$

the integrals of all subintervals can be expressed in a matrix notation:

$$\mathbf{F} = \mathbf{W_n} \cdot \mathbf{f} = \begin{bmatrix} x_2 & & x_N \\ 0, \int f(x)\,dx, \ldots, & & \int f(x)\,dx \\ x_1 & & x_{N-1} \end{bmatrix}^T_{N\times 1}$$

where the n denotes the degree of the approximating polynomial. $\mathbf{W}_n$ is a N×N weighting matrix. A sequence of integrals would be represented by:

$$F_{\mathbf{S}} = \boldsymbol{SW_n} \cdot \mathbf{f} = \mathbf{L} \cdot \mathbf{f} = \begin{bmatrix} x_2 & & x_N \\ 0, \int f(x)\,dx, \ldots, & & \int f(x)\,dx \\ x_1 & & x_1 \end{bmatrix}^T_{N\times 1}$$

where the **S** is a lower triangular summing matrix and L the integrating matrix **L**. the integrating matrix is then defined as a linear operator with the property:

$$\mathbf{f} = \mathbf{L} \cdot \mathbf{f'} + f(0)[\mathbf{1}]_{N\times 1}$$

where the boundary condition vector remains to be evaluated. Two boundary-condition matrix operators:

$$\mathbf{B}_0 = \begin{bmatrix} 1 & 0 & \cdots & 0 \\ 1 & 0 & \cdots & 0 \\ \vdots & \cdots & \cdots & \vdots \\ 1 & 0 & \cdots & 0 \end{bmatrix} \quad \text{and} \quad \mathbf{B}_1 = \begin{bmatrix} 0 & 0 & \cdots & 1 \\ 0 & 0 & \cdots & 1 \\ \vdots & \cdots & \cdots & \vdots \\ 0 & 0 & \cdots & 1 \end{bmatrix}$$

provide a series of properties that are useful in the solution of two-point boundary value problems:

$$\mathbf{B_0} \cdot \mathbf{f} = \mathbf{f}(0) = \mathbf{f}_1 \quad \text{and} \quad \mathbf{B_1} \cdot \mathbf{f} = \mathbf{f}(1) = \mathbf{f}_N \ .$$

Example:

Given a differential equation:

e.g. $Q'(x) = -m' \ddot{w}(x) + F_L'(x)$

1.) Normalisation of the differential equation:

e.g. $Q'(r) = \frac{dQ}{dr} = \frac{1}{R} \cdot \frac{dQ}{dx} = \frac{1}{R} \cdot Q'(x)$ with $x = \frac{r}{R}$

2.) Truncation:

e.g. $Q'(r) = -R\,m' \ddot{w}(r) + R\,F_L'(r)$

$\rightarrow$ $\mathbf{Q}' = -R\,\mathbf{m}' \cdot \ddot{\mathbf{w}} + R\,\mathbf{F}_L'$

3.) Integration due to multiplication with the integrating matrix L:

e.g. $\mathbf{Q} = -\mathbf{L} \cdot R\,\mathbf{m}' \cdot \ddot{\mathbf{w}} + \mathbf{L} \cdot R\,\mathbf{F}_L' + \mathbf{k}_Q$

4.) The constant of integration k_Q can be calculate by solving the boundary value problem.

$\Rightarrow$ In frequency domain ones get a linear equation system!

10. APPENDIX B - UNEVEN BLADE PROPERTIES

The referenced uneven blade properties, used for the above mentioned calculations, are shown in the following figures.

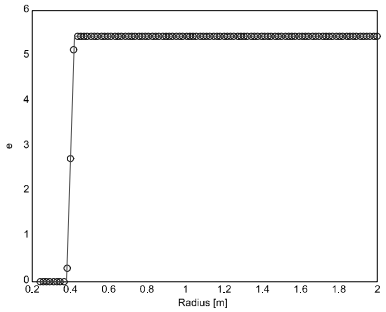

Figure B.1: Mass centroid offset from elastic axis.

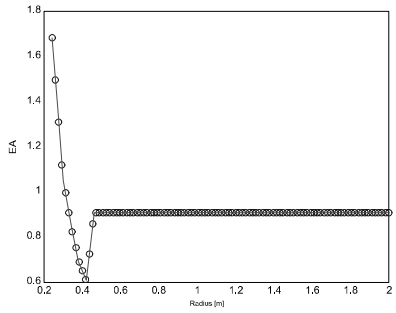

Figure B.2: Elongation stiffness per unit.

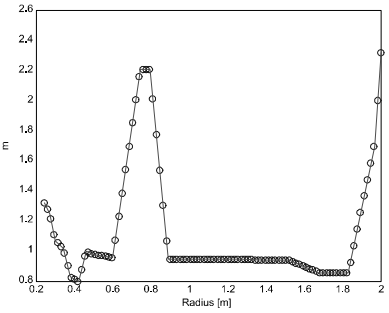

Figure B.3: Mass per unit.

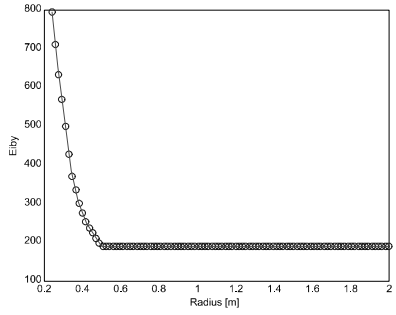

Figure B.4: Bending stiffness per unit (flap).

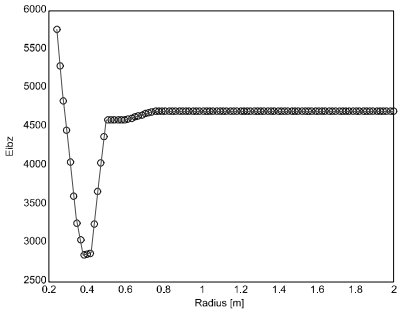

Figure B.5: Bending stiffness per unit (lead-lag).

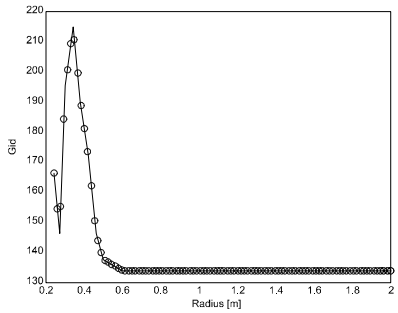

Figure B.6: Torsional stiffness per unit.

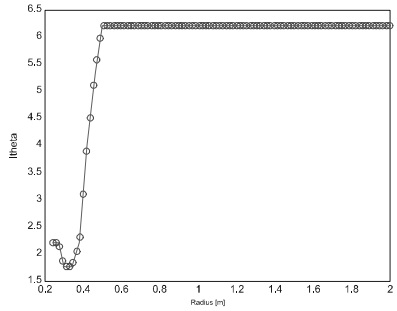

Figure B.7: Inertia mass per unit (torsion).

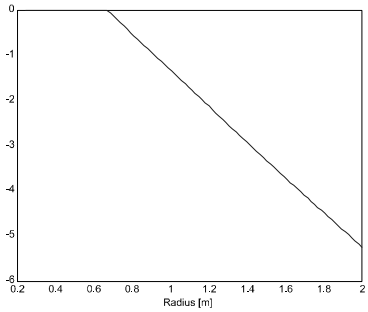

Figure B.8: Pretwist.